Nat. Volatiles & Essent. Oils, 2021; 8(4): 16052-16067

NVEO
Natural Volatiles &
Essential Oils

Investigation Of Variable Sized Silver Nanospheres Deposited On ITO/C-Si Structure As FDTD Simulation Model For Plasmonic Solar Cells

Manju Rani[1,2], Jyoti Kashyap[2], Udaibir Singh[3*], Avinashi Kapoor[2]

[1] Department of Physics, Deshbandhu College, University of Delhi, Kalkaji, New Delhi-110019, India

[2] Department of Electronic Science, University of Delhi, South Campus, Benito Juarez Road, New Delhi-110021, India

[3] Department of Electronics, Acharya Narendra Dev College, University of Delhi, Kalkaji, Govindpuri New Delhi-110019, India

*Corresponding author: udaibirsingh@andc.du.ac.in

Abstract

The adoption of metal nanoparticles has been well demonstrated for enhanced absorption in solar cells. In this work, effect of size of silver nanospheres (AgNS) deposited upon ITO (indium tin oxide)/crystalline silicon(c-Si) substrate has been investigated using MEEP software via FDTD method. Scattering efficiency enhances from 0.1% (corresponding to 30nm) to 15.6% (corresponding to 100nm) in visible region. Maximum response of transmittance at transparent conducting oxide (TCO)/semiconductor interface has been observed for 100nmAgNS. Spatial distribution of electric field intensity shows enhanced near field spectra around the nanospheres as well as in the active layer of structure.

Keywords: Plasmonics, Silver nanospheres, FDTD, Scattering, Absorption, Transmittance, Solar cell

1. Introduction

The energy demand of the world is increasing day by day. Conventional resources of the energy are limited and their contribution the global pollution is notable. Solar energy is the most reliable renewable source which provides an environment friendly solution to meet the increasing energy demands. Basic mechanism behind the conversion of solar energy into electric energy is the photovoltaic effect. In c-Si (bandgap- 1.12 eV at 300 K) based solar cells, absorption is low as silicon is not able to absorb red light out of the visible spectrum range due to its material properties [1]. Plasmonics is widely being utilized to increase the light trapping and improve the efficiency of the solar cells after first and second- generation solar cells [1,2]. Metal nanoparticles when placed on the top of dielectric/ semiconductor interface, scatter the incident photons in forward and backward directions. The photons scattered in forward direction supports the enhancement of light trapping inside the active layer of the cell which results in improved overall power conversion in solar cells [3, 4]. Enhancement of efficiency by making use of plasmonics in various types of solar cells is well

reported [5-7]. Size and shape of the nanoparticles affect their optical properties strongly which in turn modifythe light absorption and efficiency of solar cells8,9]. In recent years, use of nanostructures of dielectric materials such as SiO_2, Si_3N_4, TiO_2 and Cu_2O has also been explored for photovoltaic applications [10-13]. B. K. Mousavi et al. also explored the role of silicon nanowires for their plasmonic effect [14]. As far as, metal nanoparticles are concerned, silver nanoparticles are found to be highly efficient for solar cell applications as they offer large scattering efficiency with low absorption losses [15-17]. In the present work, effect of size of AgNS when deposited on ITO/c-Si heterojunction has been investigated in terms of scattering efficiency, electric field and transmittance.

2.Theory

2.1. Plasmonics

In metals, conduction electrons are available in large numbers which behave like electron gas. In presence of incident electromagnetic field which is alternating in nature, these charges get displaced from their position and restored back due to coulombic attraction of positive ions. This results in oscillation of the electron cloud being referred as plasma oscillations and its quantum is termed as plasmon. Applying Newton's law for single electron [18]

$$m\frac{d^2x}{dt^2} = -eE_x \qquad (1)$$

Where x is the displacement of electron and m is the effective mass of electron.

For free electron density n, the electric field E_X generated by a surface charge, nex can be found using Gauss theorem as $E_X = \frac{2nex}{2\varepsilon_0}$. Hence the bulk plasmon frequency is given by [18]

$$\omega_p = \sqrt{\frac{ne^2}{m\varepsilon_0}} \qquad (2)$$

Where ε_0 is the permittivity of free space.

Since the radius of the nanospheres is very much less than the wavelength of the incident radiation, the generated field component can be related with the uniform polarization P_X as $E_X = \frac{-P_X}{3\varepsilon_0}$. Hence the resonance frequency due to collective oscillation of the electrons can be written as [18]

$$\omega_{sp} = \frac{\omega_p}{\sqrt{3}} = \sqrt{\frac{ne^2}{3m\varepsilon_0}} \qquad (3)$$

The surface plasmon waves propagate at the interface of the metal and the dielectric. The dielectric constant (ε_r) of metals is complex in nature and very much varies with the frequency of the incident radiation as defined by Drude model and is given by [19]

$$\varepsilon_r(\omega) = 1 - \frac{\omega_p^2}{\omega^2 + i\Upsilon(\omega)\omega} \qquad (4)$$

2.2. Scattering by metal nanospheres

The conduction electrons in a metal oscillate collectively on interaction with incident electromagnetic radiation that gives rise to plasmon resonance. At wavelengths near plasmon resonance, metal nanoparticles scatter the incident light very strongly. For nano-dimensional particles where the size is very much small as compared to the wavelength of the incident radiation in visible region, the particle can be approximated as a simple dipole [1]. The scattering and absorption by spherical nanoparticles or nanospheres can be well explained by the Lorentz Mie theory. According to this theory, the cross-sections for extinction (sum of scattering and absorption cross-sections), scattering and absorption are given by following respective relations [20]:

$$C_{ext} = \frac{2\pi}{k^2}\sum_{n=1}^{\infty}(2n+1)\,Re(a_n + b_n) \quad (5)$$

$$C_{sca} = \frac{2\pi}{k^2}\sum_{n=1}^{\infty}(2n+1)\,(|a_n|^2 + |b_n|^2) \quad (6)$$

$$C_{abs} = C_{ext} - C_{sca} \quad (7)$$

where $k = \frac{2\pi N}{\lambda}$, N is refractive index of the surrounding medium and λ is the wavelength of the incident radiation. The Mie coefficients a_n and $b_n$are given by

$$a_n = \frac{m\psi_n(mka)\psi_n'(ka) - \psi_n(ka)\psi_n'(mka)}{m\psi_n(mka)\chi_n'(ka) - \psi_n(ka)\chi_n'(mka)} \quad (5)$$

$$b_n = \frac{\psi_n(mka)\psi_n'(ka) - m\psi_n(ka)\psi_n'(mka)}{\psi_n(mka)\chi_n'(ka) - m\psi_n(ka)\chi_n'(mka)} \quad (6)$$

Where ψ and χ are Riccati-Bessel functions of the first and third kind respectively, a is the radius of the nanosphere and $m = \frac{N_p}{N}$, N_p being complex refractive index of the nanosphere material. The scattering and absorption cross-sections for a metallic nanosphere have high dependence on the polarizability of the particle which is given by

$$\alpha = 4\pi a^3\left(\frac{\varepsilon_p - \varepsilon_m}{\varepsilon_p + 2\varepsilon_m}\right) \quad (7)$$

Where a is the radius of nanosphere, ε_p and ε_m are the dielectric functions of metal nanosphere and embedding medium respectively. It is obvious from expression (10) that polarizability will be very large if $\varepsilon_p = -2\varepsilon_m$. This is the condition for surface plasmon resonance [1,21].

The extinction efficiency (Q_{ext}), scattering efficiency (Q_{sca}) and absorption efficiency (Q_{abs}) for the metallic nanospheres are defined as the ratio of respective cross-sections to the geometric projection of the nanosphere on the plane perpendicular to the incident light and can be written as

$$Q_i = \frac{C_i}{\pi a^2} \qquad (8)$$

Where i may stand for extinction, scattering or absorption [20]

3. Structure for FDTD Simulation

The working principle of a photovoltaic cell resembles with that of a p-n junction diode. Electron-hole pairs are generated when the photons with energy equal to or greater than the bandgap of the semiconductor incident on the junction. Movement of these charge carriers create photocurrent through an external circuit [22,23]. The amount of photocurrent generated depends upon the wavelength of the incident radiation along with the quantum efficiency (QE) of the solar cell which in turn depends on the number of charge carriers (electron-hole pairs) generated in the active layer of the solar cell.

In this simulation model, the ITO/c-Si heterojunction is taken for investigating the effect of size of AgNS on scattering, absorption and transmission of the incident radiation. Silicon is one of the most abundant elements on the earth's crust. It is being used for fabrication and implementation of photovoltaic devices at large scale for industrial purposes. c-Si (band gap ~ 1.12 eV at 300 K) based solar cell release less toxic materials as compared to another ones (for example GaAs based solar cells) [24-26]. ITO (bandgap ~ 3.5-4.3 eV) is a transparent conducting oxide (TCO) having very high transparency (~ 92%) and conductivity (ρ = 2.2 X 10^{-4} Ω-cm) as fabricated with method discussed by Zhangxian Chen et al. [27]. ITO is a recognized n-type degenerate semiconductor which has high transmittance in near infra-red and visible regions of the electromagnetic spectrum [28,29]. Use of ITO as a highly efficient photocathode in dye-sensitized solar cell has also been reported by Ze Yu et al. [30]. MEEP is an open- source software which is used to simulate Maxwell's equations over a finite time difference [31]. In this work, Numerical simulation has been performed via FDTD method using MEEP to investigate the scattering and absorption efficiencies for three different combinations namely AgNS in air, AgNS on the top of ITO and AgNS on the top of ITO/c-Si heterojunction to demonstrate the effect of increasing size of nanosphere. Simulation has also been executed for near field spectra to show spatial distribution of electric field in Ag/ITO/c-Si structure. The transmitted power has been measured at the TCO/semiconductor interface.

The integrated transmission efficiency (ITE) can be calculated in spectral range λ_1 to λ_2 as [32]

$$\mathrm{ITE} = \frac{\int_{\lambda_1}^{\lambda_2}\left(\lambda/hc\right)[T(\lambda)]S(\lambda)d\lambda}{\int_{\lambda_1}^{\lambda_2}\left(\lambda/hc\right)S(\lambda)d\lambda} \qquad (9)$$

Where λ is the wavelength of the light in free space, h is Plank's constant, c is the speed of light in free space, $T(\lambda)$is the transmittance of light and $S(\lambda)$ is the irradiance spectrum of AM1.5G.

The dimensions of 3-D model simulation cells for the structures AgNS in air and AgNS on ITO have been taken equal to 1µm x 1µm x 1µm. The incident power source has been taken in form of a Hz polarized Gaussian source extended in X-Z plane across the boundaries. and directed in Y direction. The source is equivalent to the AM1.5G solar spectrum and range of wavelength was set from 300 nm to 800 nm in the visible spectrum. To reduce the computational time, mirror symmetry along X-axis has been considered. Optical constants for modelling c-Si, Ag and ITO were taken from the literature [32,33]. The simulation for all the three structures has been executed separately. The 2-D cross-sectional schematic diagrams of the simulation cells with position of source and flux monitors for AgNS in air and AgNS on the top of ITO are shown in Fig.1(a) and Fig.1(b) respectively.

4. Plasmonic Solar Sell Model

The structure under investigation for plasmonic solar cell application is designed as AgNS upon ITO film (thickness 100 nm) layered above c-Si substrate with silver back contact. A 3-D schematic diagram of the structure and 2-D cross-sectional view of simulation cell are shown in fig. 2(a) and 2(b) respectively. The

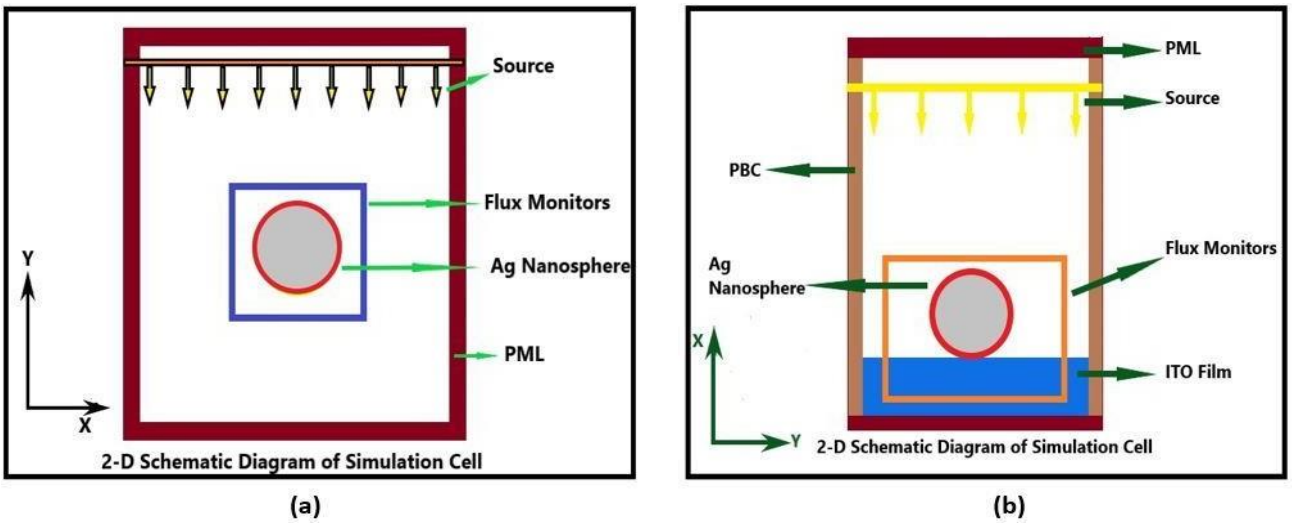

Fig. 1. Two-dimensional cross-sectional schematic diagram of simulation cell for (a) AgNS in air (b) AgNS on ITO.

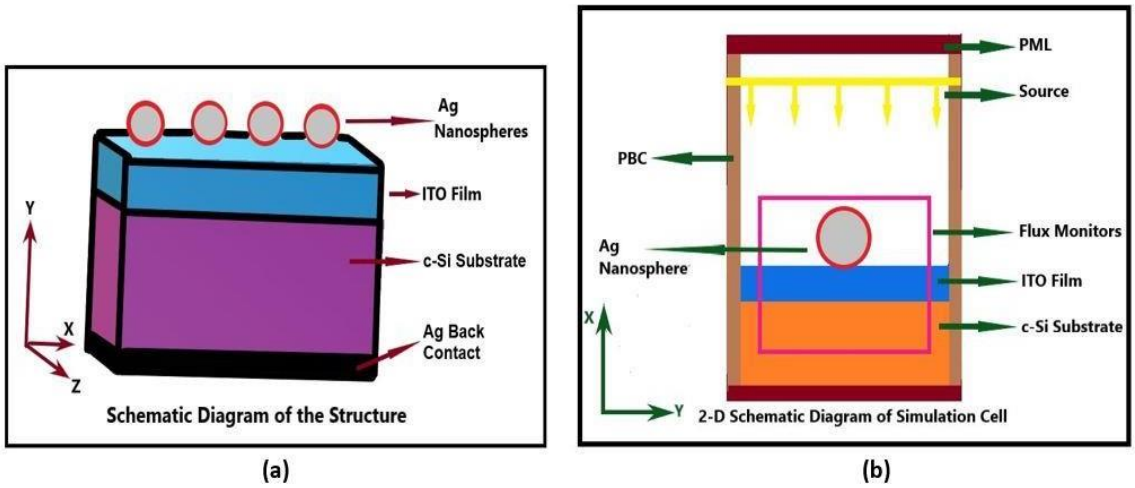

Fig. 2. Three-dimensional schematic diagram of the structure for plasmonic solar cell (b) Two-dimensional cross-sectional schematic diagram of simulation cell for AgNS/ITO/c-Si structure.

dimensions of the simulation cell have been taken 1µm x 2.2 µm x 1 µm. The incident power Gaussian source equivalent to AM1.5G is placed near the uppermost PML. Periodic boundaries were used to make the structure periodic. The flux monitors have been placed around the structure for simulation. Simulations have been executed for efficiencies (scattering, absorption and extinction), x- component of electric field (E_x) and transmittance of the incident radiation into the substrate for the AgNS having diameters in 30nm-100nm range.

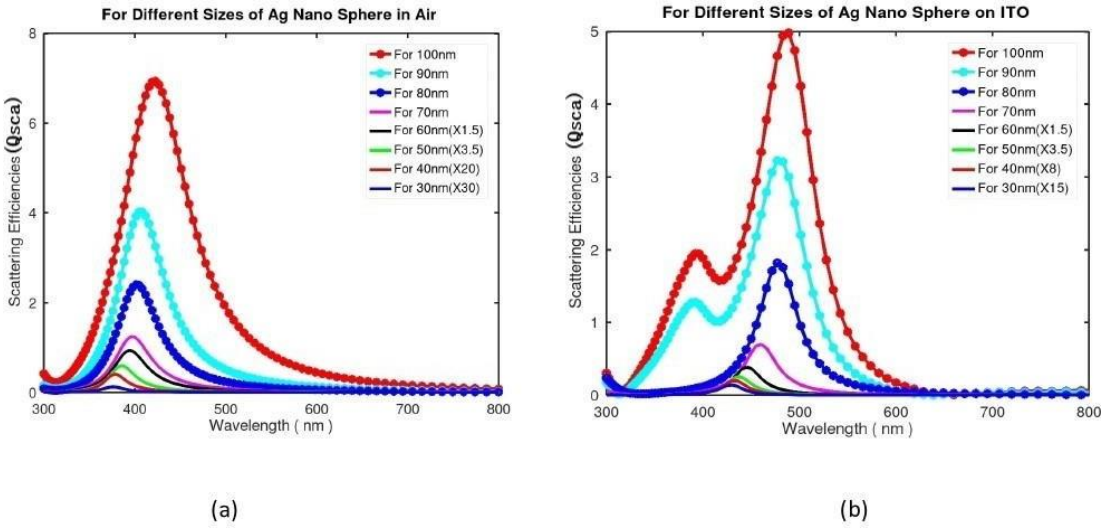

Fig. 3. Variation of scattering efficiencies, Q_{sca} with wavelength for (a) AgNS (30nm to 100nm) in air. Efficiencies for 30nm to 60nm AgNS are multiplied by a factor shown in inset for better resolution (b) AgNS (30nm to 100nm) deposited on ITO. Efficiencies for 30nm to 60nm AgNS are multiplied by a factor shown in inset for better resolution.

5. Results and Discussion

Fig.3(a) shows the variation of scattering efficiency for AgNS of different sizes (30nm to 100 nm) in air within the spectral range 300nm to 800nm. An increase in scattering efficiency has been observed with the increase in size of the nanosphere. At plasmon resonance, the scattering cross section becomes much larger as compared to the geometric cross-section of the nanosphere, hence they scatter more of the incident radiation. With increase in size of the nanosphere, the conduction electrons move out of phase and depolarization occurs. This results in reduction of the field generated due to polarization of surrounding matter [1]. For 30nm Ag nanosphere, resonance peak appears at λ = 376.3nm while for 100nm Ag nanosphere, the peak shifts to λ = 422.4nm. Hence, a red shift is observed in the position of plasmon resonance peak.

When the FDTD simulation is executed for AgNS of different sizes placed on the ITO film, the variation of scattering efficiencies with wavelength has been shown in Fig.3(b). The effect of interaction between nanospheres and TCO is clearly visible in this figure. Appearance of higher order resonance peak has been observed for larger size nanospheres due to dynamic depolarization and radiative damping effects [1].

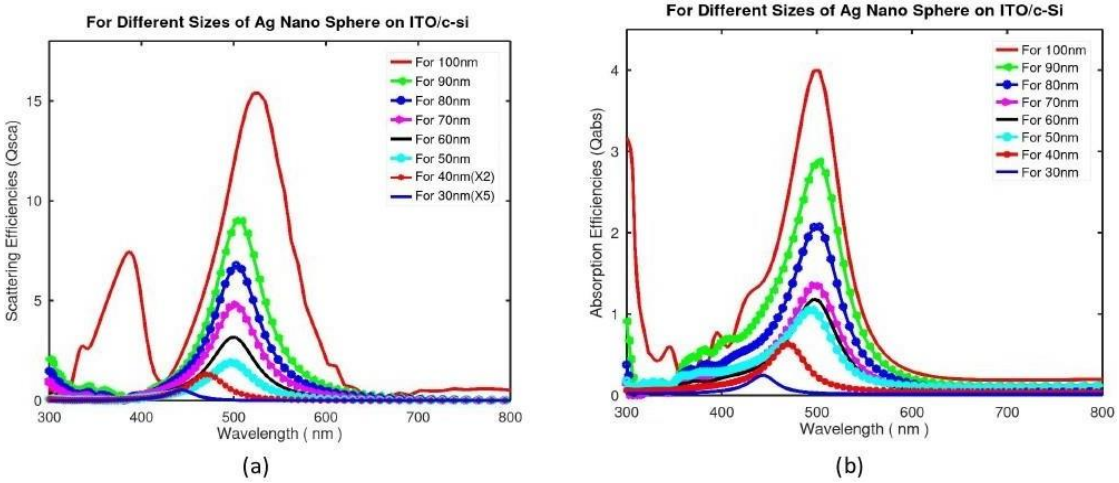

Fig. 4. Variation of (a) scattering efficiencies, Q_{sca} with wavelength for AgNS deposited on ITO/C-Si structure (efficiencies for 30 nm and 40 nm AgNS are multiplied by a factor shown in inset for better resolution) (b) absorptionefficiencies, Q_{abs} with wavelength for AgNS deposited on ITO/C-Si structure.

However, the magnitude of scattering decreases slightly which is in accordance with the results discussed by Gursoy B Akguc [34]. This shows a significant change in the spectral response of the AgNS while they interact with ITO. For the structure under investigation, variation in the scattering efficiencies with wavelength is shown in Fig.4 (a). For larger sizes of Ag nanosphere, higher order resonance peaks appear due to quadrupole resonance [1]. An increase in scattering efficiency has been observed with a maximum of 15.6% for 100nm Ag nanosphere with maximum red shift in the resonance peak (λ_{pr}) at 529.5nm. For solar cell applications, scattering of the incident radiation by the nanospheres must exceed the parasitic absorption by the nanospheres. Fig.4(b) shows the variation of absorption efficiencies with wavelength for the different sizes of

nanospheres. The extinction efficiencies with their components scattering and absorption efficiencies for each size of Ag nanosphere are shown from Fig.5(a) to 5(h). It is found from these results that for 30 nm, the absorption by nanosphere is much large as compared to scattering but as the size of nanosphere increases, scattering becomes more significant than this parasitic absorption which is an advantage for plasmonic solar cell purpose.

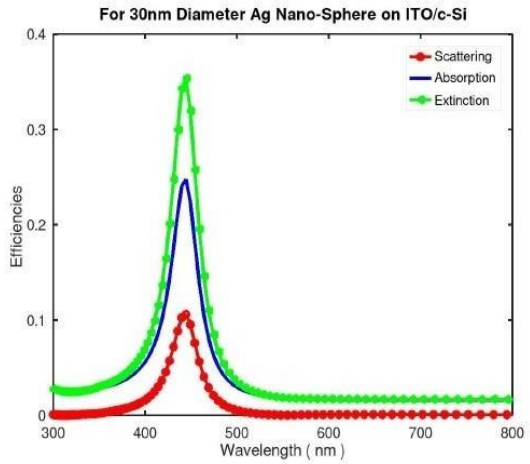

(a)

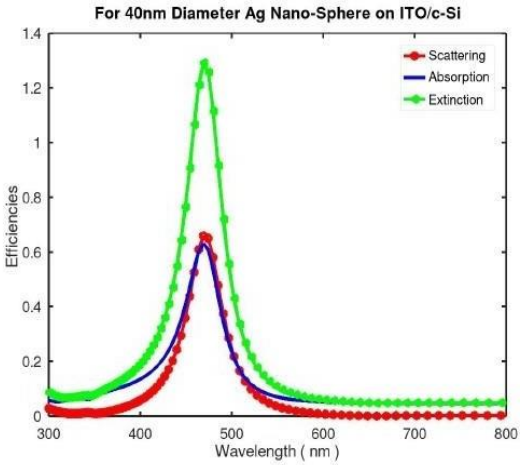

(b)

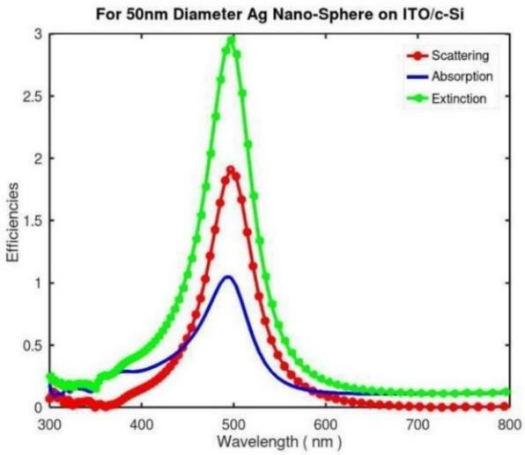

(c)

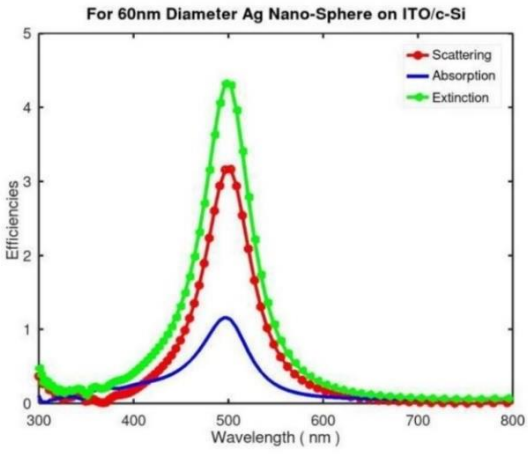

(d)

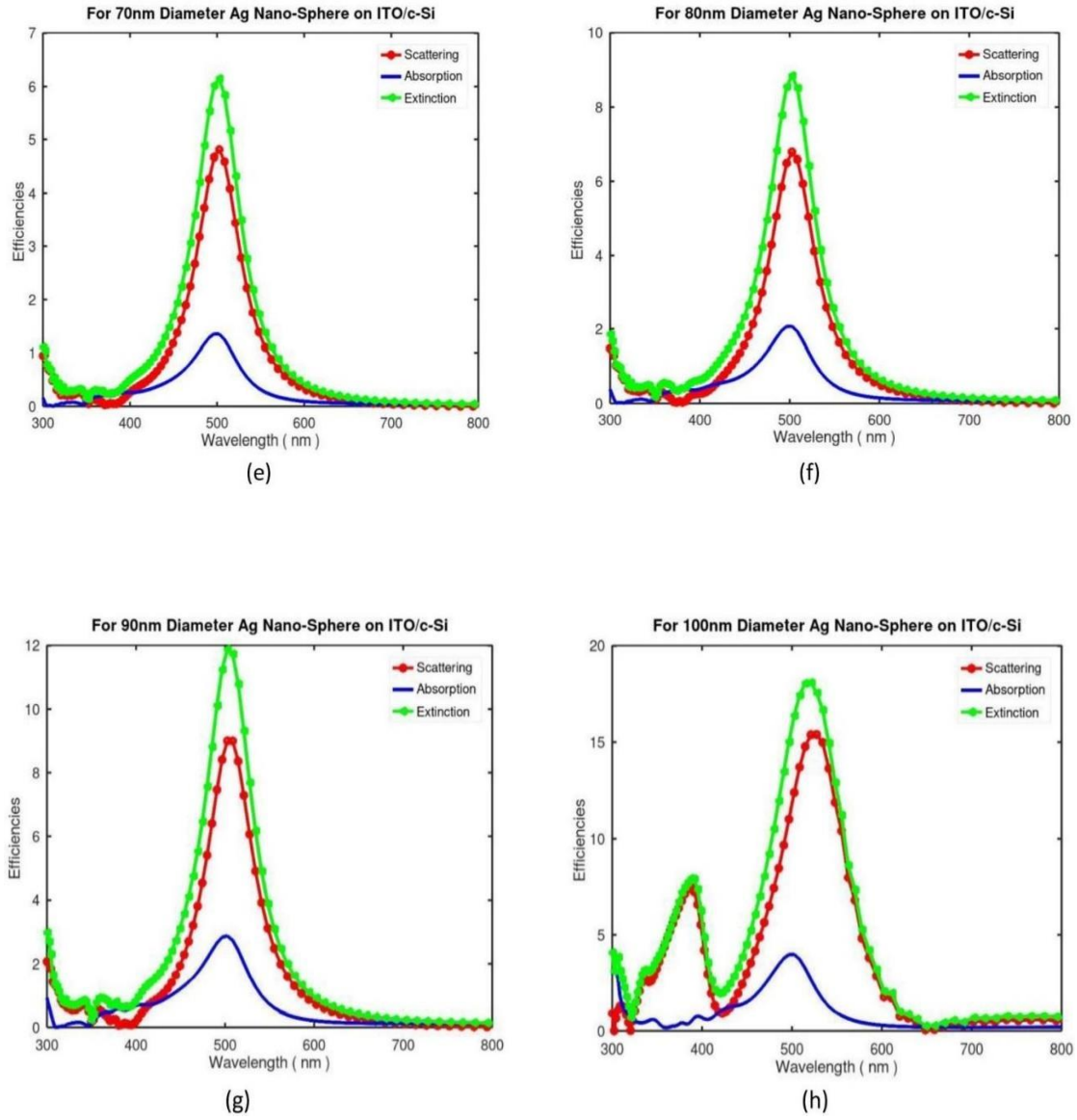

Fig. 5. Variation of Efficiencies Q_{sca}, $Q_{abs}$and $Q_{ext}$with Wavelength for AgNS/ITO/c-Si structure for (a) 30nm, (b) 40nm, (c) 50nm, (d) 60nm, (e) 70nm, (f) 80nm, (g) 90nm, (h) 100nm sizes.

Variation of extinction efficiencies and plasmonic resonant wavelength, λ_{pr} with the size of the AgNS are shown in Fig. 6(a) and 6(b) respectively. An enhancement in the magnitude of these parameters has been displayed graphically in these figures.

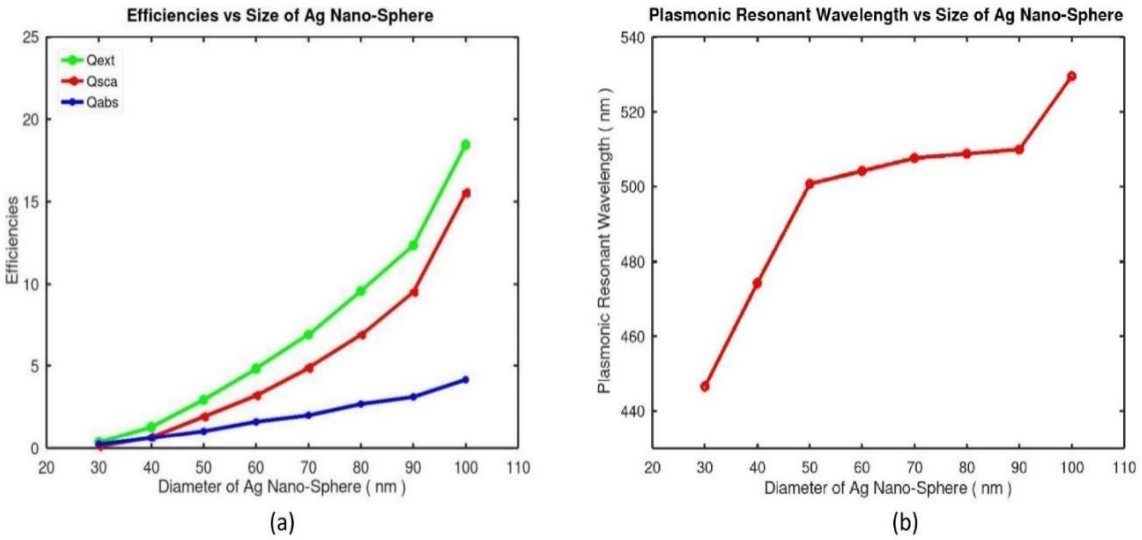

Fig. 6. Variation of (a) efficiencies Q_{sca}, $Q_{abs}$and $Q_{ext}$with different sizes of AgNS (30nm to 100nm) on ITO/c-Si structure (b) plasmonic resonant wavelength (λ_pr) with different sizes of AgNS (30nm to 100nm) on ITO/c-Si structure

Diameter of Nanosphere (nm)	Q_{ext} (%)	Q_{sca} (%)	Q_{abs} (%)	λ_{pr} (nm)
30	0.35	0.1	0.25	446.5
40	1.3	0.7	0.6	474.2
50	2.9	1.9	1.0	500.7
60	4.4	3.2	1.2	504.2
70	6.2	4.7	1.5	507.6
80	8.9	6.8	2.1	508.8
90	11.9	9.1	2.8	509.9
100	18.2	15.6	2.6	529.5

Table 1. Representation of the various components of efficiency with plasmonic resonant wavelength for different sizes of Ag nanospheres on ITO/c-Si substrate

Table 1 shows a comparative representation of the variation of extinction, scattering and absorption efficiencies with wavelength for different sizes of AgNS deposited on ITO/c-Si substrate. Corresponding plasmonic resonant wavelength is also represented. Extinction efficiency is maximum for 100nm Ag nanosphere (18.2%) with a maximum scattering efficiency of 15.6%. Plasmonic resonant wavelength has also been found maximum (529.5 nm) for this size of AgNS.

Diameter of Nanosphere (nm)	Q_{sca} (As Fractional % of Q_{ext})	Q_{abs} (As Fractional % of Q_{ext})
30	28.5	71.5
40	53.8	46.2
50	65.5	34.5
60	72.7	27.3
70	75.8	24.2
80	76.4	23.6
90	76.5	23.5
100	85.7	14.3

Table 2. Representation of scattering and absorption efficiencies as % fraction of total extinction efficiency

Table 2 shows the fractional distribution of scattering and absorption efficiencies out of the total extinction efficiency for different sizes of the AgNS deposited on ITO/c-Si substrate. For 30nm Ag nanosphere, almost 72% of the total extinction radiation has been absorbed by the nanosphere while around only 28% is scattered. Maximum fractional scattering efficiency has been found for 100 nm Ag nanosphere which is almost equal to 86%.

In plasmonic nanostructures, the surface plasmon and localized surface plasmon have been observed for the TM polarization (magnetic field perpendicular to the direction propagation) of the incident radiation [35].

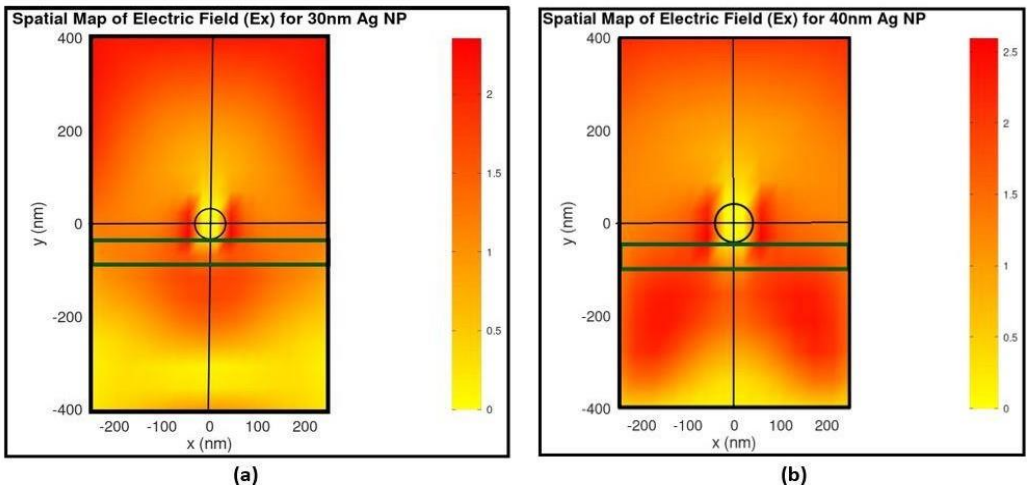

(a) (b)

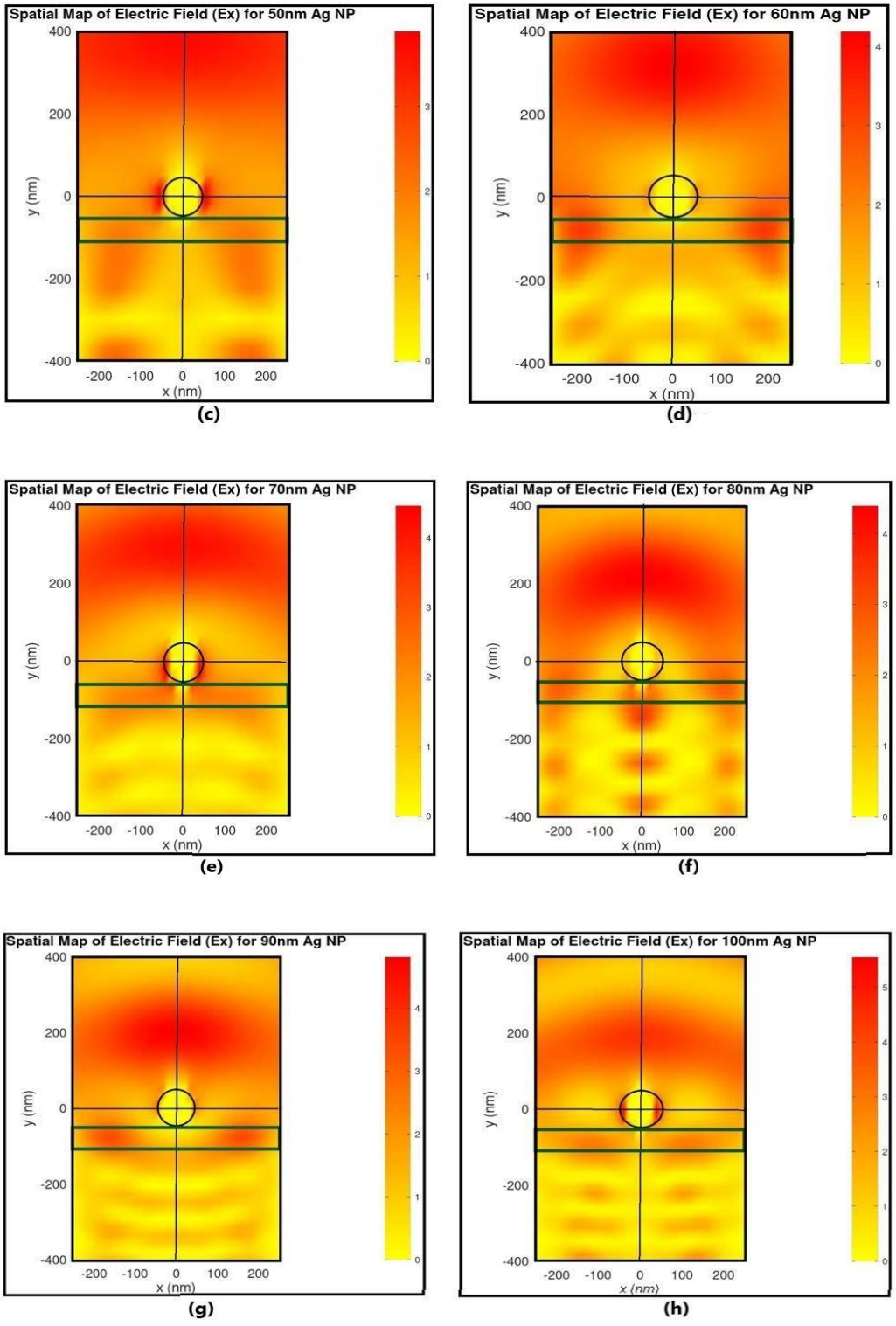

Fig..7. Spatial distribution of electric field intensity for Ag/ITO/c-Si structure simulated at corresponding plasmonic resonant wavelengths for (a) λ_{pr} = 446.5nm for 30nm diameter, (b) λ_{pr} = 474.2nm for 40nm diameter, (c) λ_{pr} = 500.7nm for 50nm diameter, (d) λ_{pr} = 504.2nm for 60nm diameter, (e)λ_{pr}= 507.6nm for 70nm diameter, (f) λ_{pr} = 508.8nm for 80nm diameter, (g)λ_{pr}= 509.9nm for 90nm diameter, (h) λ_{pr} = 529.5nm for 100nm diameter

Hence, electric field along the TCO/semiconductor interface imparts significant contribution for generation of charge carriers. Electric field (E_x component) has been investigated for different sizes of AgNS at plasmon excitation corresponding to the plasmonic resonant wavelength, λ_{pr}. Figures 7(a) to 7(h) show the spatial distributionof the electric field intensity with corresponding colour bar. The colour bar indicates the intensity of the electric field in the Ag nanosphere/ ITO/c-Si structure. This gives an impression about enhancement of electricfield at excitation of surface plasmons. An enhancement in electric field inside the active layer has been observed with theincreasing size of the nanosphere.

Transmission spectra at TCO/semiconductor interface for various sizes of AgNS is shown in Fig.8. For reference, simulation has been executed for the structure without nanospheres. An increase in transmittance for a particular size of nanosphere is observed at wavelengths

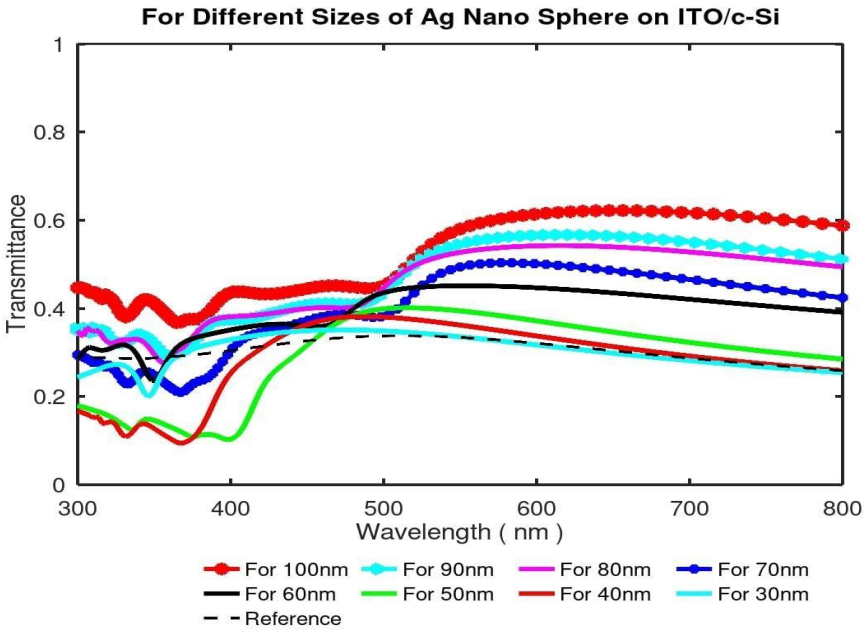

Fig. 8. Variation of transmittance with wavelength at metal/TCO interface in Ag/ITO/c-Si structure for different sizes (30nm to 100nm) of Ag nanospheres

above resonance. This happens due to the constructive interference between the incident light and the forward scattered light by the nanospheres [36,37]. Further, higher transmittance is observed with the increasing size of the nanosphere with a maximum for 100 nm diameter.

6. Conclusion

Effect of variation in AgNS size on scattering, absorption, transmission and electric field intensity in AgNS/ITO/c-Si structure has been investigated numerically using MEEP via FDTD method. The plasmonic resonance gets shifted towards the infra-red region of the electromagnetic spectrum and broadening of resonance peak is also observed with the increasing size of AgNS. This red shift and broadening in resonance peak impart enhanced light trapping in the active layer of the solar cell. Scattering efficiency increases from 0.1% to 15.6% as the size of AgNS increases from 30nm to 100nm. For 30 nm AgNS, scattering and absorption by the nanosphere are almost 28% and 72% (as a fraction of total extinction efficiency) respectively, which is a significant loss of the incident radiation. As the size of the nanosphere increases, scattering increases and overcomes this parasitic absorption gradually. For 100 nm AgNS, fraction of scattering becomes almost 85% while that of absorption reduces to almost 15% which is a remarkable enhancement for plasmonic solar cell applications. Also, enhanced transmission into the c-Si substrate has been detected for this size of AgNS with reference to the FDTD simulation results for structure without AgNS. Thus, amongst the various sizes of AgNS studied, 100 nm proves to be an optimised size to yield the highest efficiency due to enhancement in broadband light coupling. This work is capable to become a fundamental study for reasonable improvement of efficiency in silicon based plasmonic solar cells with ITO used as photocathode.

References

[1] Catchpole K R, Polman A. Plasmonic solar cells. Optics Express.2008;**16**(26): 21793-21800.

[2] Ferry V E et al. Plasmonic nanostructure design for efficient light coupling into solar cells. Nano Letters.2008; **8(12):** 4391-4397.

[3] Spinelli P et al. Plasmonic light trapping in thin-film solar cells. Journal of Optics.2012;**14:** 1-11.

[4] Tian Y, Tatsuma T. Mechanisms and applications of plasmon-induced charge separation at TiO_2 films loaded with gold nanoparticles. J. Am. Chem. Soc. 2005;**127(20):** 7632-7637.

[5] Singh G, Verma S S. Enhanced efficiency of thin film GaAs solar cells with plasmonic metal nanoparticles. Energy Sources, Part A: Recovery, Utilization, and Environmental Effects. 2017; DOI: 10.1080/15567036.2017.1407840

[6] Wang Y, Liu Q, Zhang W Cet al. Analysis of light trapping effect of thin film solar cell based on surface plasmon wave induced by metal nano-grating. Integrated Ferroelectrics.2016;170(1):137-145,

[7] Shoukat I M, Ayub A et al. Perovskite solar cells: importance, challenges, and plasmonic enhancement. International Journal of Green Energy.2020; DOI:10.1080/15435075.2020.1818567.

[8] Mohapatra S, Mishra Y K, Warrier A M et al. Plasmonic, low-frequency Raman, and nonlinear optical-limiting studies in copper-silica nanocomposites. Plasmonics.2012; **7 (1)**: 25-31.

[9] Li S, Zhu X, Wang B et al. Influence of Ag nanoparticles with different sizes and concentrations embedded in a TiO_2compact layer on the conversion efficiency of perovskite solar cells, nanoscale research letters.2018;**13**:210.

[10]Akimov Y A, Koh W S, Sian S Y et al. Nanoparticle-enhanced thin film solar cells: Metallic or dielectric nanoparticles? Appl. Phys. Lett. 2010; **96**: 073111 doi: 10.1063/1.3315942.

[11]James R N, Scarpulla MA. Enhanced absorption in optically thin solar cells by scattering from embedded dielectric nanoparticles. Optics Express. 2010; A139-A146.

[12]Abdelfatah M, Ismail W, El-Shafai N M et al. Effect of thickness, bandgap, and carrier concentration on the basic parameters ofCu2O nanostructures photovoltaics: numerical simulation study. Materials Technology. 2020; DOI: 10.1080/10667857.2020. 1793092

[13]Nayef U M, Hubeatir K A, Abdulkareem Z J. Characterisation of TiO_2 nanoparticles on porous silicon for optoelectronics application. Materials Technology.2016; DOI: 10.1080/10667857.2015.1132988.

[14]Mousavi B K, Silani Y, Talarposhti M R. Formation of highly luminescent strained silicon nanowires due to surface effects and possible Plasmon role. Materials Technology.2020; DOI: 10.1080/10667857.2020.1806607.

[15]Deka N, Islam M, Sarswat P K et al. Enhancing solar cell efficiency with plasmonic behavior of double metal nanoparticle system. Vacuum. 2018; **152**:285-290.

[16]Ouyang Z, Zhao X, Varlamov S et al. Nanoparticle enhanced light trapping in thin-film silicon solar cells. Prog. Photovoltaics Res.Appl.2011;**19(8):**917-926.

[17]Yang Y, Pillai S, Mehrvarz H et al. Enhanced light trapping for high efficiency crystalline solar cells by the application of rear surface plasmons. Sol. Energy Mater. Sol. Cell.2012; 101.

[18]Sarkar P, Maji B, Aritra et al. Effect of surface plasmon-based improvement in optical absorption in plasmonic solar cell. International Journal of Nanoscience.2017;**16(4):** 1760028-1-1760028-7.

[19]Sarkar P, Panda S, Maji B et al. Study on surface plasmon-based improvement in absorption in plasmonic solar cell. International J Nanoparticles.2018;**10 (½):** 77-91.

[20]Paris A et al. Plasmonic scattering by metal nanoparticles. Plasmonics.2012; **7** 525-34

[21]Gangadharan D T et al. Recent advancements in plasmon-enhanced third-generation solar cells. Nanophotonics.2017;**6 (1):**153-175.

[22]Gray J L. The physics of solar cell. Handbook of photovoltaic science and engineering. John Wiley and sons ltd.2011; 82-129.

[23]Yoshikawa K et al. Silicon heterojunction solar cell with interdigitated back contacts for a photoconversion efficiency over 26%. Nature Energy.2017;**2:** 17-032

[24]Sze S M, Irvin J C. Resistivity, mobility and impurity levels in GaAs, Ge, and Si at 300^{o}K.Solid State Electronics.1968; **11(6):** 599-602

[25]Omura M et al. Testicular toxicity of gallium arsenide, indium arsenide, and arsenic oxide in rats by repetitive intratracheal instillation. Toxicological Sciences.1996;**32(1):** 72-78

[26]Hong Y S, Song K H, Chung J Y et al. Health effects of chronic arsenic exposure. Journal of Preventive Medicine and Public Health.2014; **47(5):**245.

[27]Chen Z, Li W, Li R et al. Fabrication of highly transparent and conductive indium–tin oxide thin films with a high figure of merit via solution processing. Langmuir. 2013;**29**: 13836−13842.

[28]Kim H, Gilmore C M, Pique A et al. Electrical, optical, and structural properties of indium-tin-oxide thin films for organic light-emitting devices. J. Appl. Phys.1999; **86**:6451–6461.

[29]Hamberg I, Granqvist C G, Berggren K F et al. Band-gap widening in heavily Sn-doped In_2O_3. Phys. Rev. B.1984; **30:** 3240–3249.

[30]Yu Z, Perera I R, Daeneke T et al. Indium tin oxide as a semiconductor material in efficient p-type dye-sensitized solar cells.NPG Asia Materials. 2016;**8**: e305.

[31]Oskooi A F, Roundy D, Ibanescu M et al. MEEP: A flexible free-software package for electromagnetic simulations by the FDTD method. Computer Physics Communications. 2010;**181:** 687-702.

[32]Singh Y P, Jain A, Kapoor A. Localized surface plasmons enhanced light transmission into c-silicon solar cells. Journal of Solar Energy.**2013** 584283.

[33]Palik E. Handbook of optical constants of solids. Academic Press. 1985; Elsevier Science 350-356.

[34]Akguc G B. Silver nanoparticles plasmonic response in the proximity of an interface. Aspects of Nanotechnology. 2019;**2(1):**61-69.

[35]Radder C, Satyanarayana B S. FDTD based plasmonic light trapping analysis in thin film hydrogenated amorphous silicon solar cells. International Journal of Renewable Energy Research.2017;**8(1):** 514-522.

[36]Beck F J, Polman A, Catchpole K R et al. Tunable light trapping for solar cells using localized surface plasmons. Journal of Applied Physics.2009;**105:** 114310-1-114310-7.

[37]Spinelli P, Lare C V, Verhagen E et al. Controlling Fano line shapes in plasmon-mediated light coupling into a substrate. Optics Express. 2011;**19:** A303-A311.